Functional ultrasound imaging of stroke in awake rats.

Clément Brunner[1,2,3,4], Gabriel Montaldo[1,2,3,4], Alan Urban[1,2,3,4]

[1] Neuro-Electronics Research Flanders, Leuven, Belgium.
[2] Vlaams Instituut voor Biotechnologie, Leuven, Belgium.
[3] Interuniversity microelectronics centre, Leuven, Belgium.
[4] Department of neurosciences, KU Leuven, Leuven, Belgium.

Correspondence should be addressed to Alan Urban (alan.urban@nerf.be).

Abstract

Anesthesia is a major confounding factor in preclinical stroke research as stroke rarely occurs in sedated patients. Moreover, anesthesia affects both brain functions and the stroke outcome acting as neurotoxic or protective agent. So far, no approaches were well suited to induce stroke while imaging hemodynamics along with simultaneous large-scale recording of brain functions in awake animals. For this reason, the first critical hours following the stroke insult and associated functional alteration remain poorly understood. Here, we present a strategy to investigate both stroke hemodynamics and stroke-induced functional alterations without the confounding effect of anesthesia, i.e., under awake condition. Functional ultrasound (fUS) imaging was used to continuously monitor variations in cerebral blood volume (CBV) in +65 brain regions/hemisphere for up to 3hrs after stroke onset. The focal cortical ischemia was induced using a chemo-thrombotic agent suited for permanent middle cerebral artery occlusion in awake rats, and followed by ipsi- and contralesional whiskers stimulation to investigate on the dynamic of the thalamo-cortical functions. Early (0-3hrs) and delayed (day 5) fUS recording enabled to characterize the features of the ischemia (location, CBV loss), spreading depolarizations (occurrence, amplitude) and functional alteration of the somatosensory thalamo-cortical circuits. Post-stroke thalamo-cortical functions were affected not only early after the stroke onset but were also altered secondarly and remotely from the initial insult. Overall, our procedure enables early, continuous, and chronic evaluations of hemodynamics and brain functions which, combined to stroke or other pathologies, aims to better understand physiopathologies toward the development of clinically relevant therapeutic strategies.

Keywords

Awake rat,
Functional diaschisis,
Functional ultrasound imaging,
Ischemic stroke,
Thalamo-cortical circuit.

Introduction

Stroke is a multifaceted and multiphasic pathology, complex to mimic under experimental conditions. Indeed, when compared to clinic, preclinical stroke models suffer from several limitations that narrow the experimental focus to few conditions[1–3]. Among these limitations, one can highlight the complexity to combine (i) imaging stroke in conscious animal models, (ii) addressing post-stroke brain functions and (iii) recording of hyperacute stroke hemodynamics, all crucial to design timely effective therapeutic strategies.

As first limitation, the use of anesthesia in preclinical studies seems to hamper the transition from animal to patient as stroke rarely occurs in sedated patients. Moreover, anesthetics disrupt the brain functionality, alterates neurovascular coupling[4,5] and affects the stroke by acting as neurotoxic or neuroprotective agents[6,7]. To date, only a few groups succeeded in inducing a stroke in awake rodents[8–11]. Moreover, post-stroke network and functional alterations have been addressed by few preclinical studies, providing evidence of functional network reorganization from minutes[12,13] to days[14–17] following stroke onset. However, these studies mostly focused on the cortical readouts and were unable to capture how deeper brain regions, like thalamic relays, were functionally and/or temporally affected remotely from the stroke insult (e.g., diaschisis)[18–20]. Furthermore, these studies were always conducted using various anesthetics (e.g., ventilated with halothane or isoflurane; medetomidine, urethane) known to differentially impact brain functions, as mentioned above.

Until recently, live monitoring of the hyperacute stroke-induced hemodynamics was restricted to few methods but often focused to the brain surface[10,21,22]. On the other hand, functional ultrasound (fUS), a recent neuroimaging modality measuring cerebral blood volume changes (CBV)[23,24], was successfully employed to measure brain functions of awake rodents[25–28], to address early post-stroke functional reorganization[13], and to track stroke-induced hemodynamics at the brain-wide scale (i.e., ischemia and spreading depolarization)[29]. However, no study has further exploited such strategies to combine together stroke hemodynamics and brain-wide functional alteration in awake rodents.

In this study, we report on the stroke induction and the alteration of somatosensory brain functions in awake rats. Using the latest improvements toward imaging of awake rodents[25–27] combined with chemo-thrombotic agent directly applied to the middle cerebral artery (MCA)[30,31], we were able to induce MCA occlusion (MCAo) in awake rats while capturing continuous hemodynamic changes, including ischemia and spreading depolarization, in +65 brain regions for up to 3hrs after stroke onset. Finally, we investigated on how somatosensory thalamo-cortical functional reponses were progressively altered from early (0-3hrs) to late post-stroke (5d) timepoints.

Materials and methods

Animals

The experimental procedures were approved by the Committee on Animal Care of the Katholieke Universiteit Leuven, following the national guidelines on the use of laboratory animals and the European Union Directive for animal experiments (2010/63/EU). The manuscript was written according to the ARRIVE Essential 10 checklist for reporting animal experiments[32]. Adult male Sprague-Dawley rats weighed between 250–400g (n=9; Janvier Labs, France) were used. During habituation rats were housed two per cage kept in a 12-hr dark/light cycle at 23°C with *ad libitum* access to water and controlled access to food (15g/rat/day). After the initial surgical procedure, rats were housed alone. See **Supplementary Table 1** reporting on animal use, experimentation, inclusion/exclusion criteria.

Body restraint and head fixation.

Rats were habituated to the workbench and to be restrained in a sling suit (Lomir Biomedical inc, Canada), progressively increasing the restraining period from minutes to hours[33,34]. After the headpost implantation (see below), rats were habituated to be head-fixed while restrained in the sling. The period of fixation was progressively increased from minutes to hours. Water and food gel (DietGel, ClearH_2O, USA) were provided along the habituation session. Once habituated, the cranial window for imaging was performed as described below (**Figure 1A-C**).

Surgical procedures

Cranial window over the MCA: Rats were anesthetized with isoflurane (5% for induction, 2% for maintenance; Iso-Vet, 1000 mg/g, Dechra, Belgium) and fixed in a stereotaxic frame. The depth of anesthesia was confirmed by the absence of reflex during paw pinching. After scalp removal and tissue cleaning, a 1-mm^2 cranial window was performed at coordinates bregma +2mm and lateral 7mm, over the left distal branch of the MCA as reported in Brunner, Korostelev et al.[13]. A silicone plug (Body Double-Fast Set, Smooth-on, Inc., USA) was used to protect the window and ease the access to the MCA before the occlusion procedure. Then, a stainless-steel custom designed headpost was fixed with bone screws (19010-00, FST, Germany) and dental cement (Super-Bond C&B, Sun Medical Co., Japan) to the animal skull (**Figure 1B,** left) as previously described by Brunner, Grillet et al.,[27].

Cranial window for imaging: After recovery and habituation to head-fixation, a second cranial window was performed between bregma -2 to -4mm and 6mm apart from the sagittal suture (same anesthesia settings as the first cranial window; see above) following the procedure described in Brunner, Grillet et al.,[28] (**Figure 1B,** right). A silicone plug was also used to protect the window and a headshield was added to secure it[25].

For both cranial windows, the dura mater was kept intact. After each surgery, rats were placed in their home cage and monitored until they woke up. Rats were medicated with analgesic (Buprenorphine, 0.1mg/kg, Ceva, France), anti-inflammatory (Dexamethasone, 0.5mg/kg, Dechra, Belgium) drugs injected directly after the surgery, at 24hrs and 48hrs after the surgery. An antibiotic (Emdotrim, 5%, Ecuphar, The Netherland) was added to the water bottle.

Chemo-thrombotic stroke induction with ferric chloride solution.

Once body restrained and head-fixed the silicone plug covering the MCA window was removed allowing the application of a drop of 20% ferric chloride solution ($FeCl_3$; Sigma Aldrich, USA) to the MCA[30,31] (**Figure 2**). Once the ischemia was visually detected using the real-time display of µDoppler images, the solution was washed out with saline to stop the reaction.

Whisker stimulation paradigm.

Two stimulation combs individually controlled by a stepper motor (RS Components, UK) were used to deliver mechanical 5-Hz sinusoidal deflection of ~20° of amplitude for 5s, alternatively to left and right whisker pads. For each whisker pad, trials were spaced by a 1.3-min period without stimulation. The blocks of stimulation were continuously delivered throughout the imaging sessions, time-locked with the fUS acquisition (**Figure 3**) to allow the subsequent analysis of hemodynamic responses within the fUS time-series.

Functional ultrasoung imaging acquisition.

Coronal µDoppler images were acquired using a 15-MHz linear probe composed of 128 piezo-elements spaced by 100µm (L22-14Vx, Vermon, France) connected to a dedicated ultrasound scanner (Vantage 128, Verasonics, USA) and controlled by a high-performance computing workstation (fUSI-2, AUTC, Estonia). This configuration allowed to image the brain vasculature with a resolution of 100µm laterally, 110µm in depth, and 300µm in elevation[28]. The ultrasound sequence generated by the software is the same as in Macé et al.,[26] and Brunner, Grillet et al.,[28]. Briefly, the ultrafast scanner images the brain with 5 tilted plane-waves (-6°, -3°, +0.5°, +3°, +6°) at a 10-kHz frame rate. The 5 plane-wave images

are added to create compound images at a frame rate of 500Hz. Each set of 250 compound images is filtered to extract the blood signal. Finally, the intensity of the filtered images is averaged to obtain a vascular image of the rat brain at a frame rate of 1.25Hz. Then, the acquired images are processed with a dedicated GPU architecture, displayed in real-time for data visualization, and stored for subsequent off-line analysis[28].

Control sessions lasted between 2.5hrs (Rat#1) and 4hrs (Rat#5,8,9). Continuous imaging session combining pre-stroke, MCA occlusion and early post-stroke recording consisted in 4hrs recording (Rat#2-4, 6-9) and late post-stroke recordings were 2 sessions of 1hr (Rat#6,8) performed 5d after the stroke onset. See **Supplementary Table 1** reporting on animal use, experimentation, inclusion/exclusion criteria.

fUS data processing and analysis

The data processing was performed following the procedure described by Brunner, Grillet et al.,[28].

Registration to Paxinos rat brain atlas and data segmentation

We registered the fUS dataset to a custom digital rat brain atlas used in Brunner et al.[29] and with one coronal plane (bregma -3.4mm) from the stereotaxic atlas of Paxinos[35]. Briefly, a spatial transformation matrix was computed on the imaged coronal cross-section that was manually aligned on the atlas by affine transformation (i.e., translation, rotation, and scaling). The dataset was segmented into 69 anatomical regions/hemisphere listed following the major anatomical structures (see **Supplementary Table 2**). The software for data registration and segmentation is open-access[36].

Relative cerebral blood volume (rCBV)

We used the relative cerebral blood volume (rCBV, expressed in % as compared to baseline) to analyze ischemia, spreading depolarizations (SDs) and functional changes. rCBV is defined as the signal in each voxel compared to its average level during the baseline period. After registration and segmentation, the rCBV signal was averaged in each individual region.

Analysis of stroke hemodynamics

The extraction of the temporal traces from the ischemic area and the SDs was performed based on the temporal analysis of the rCBV signal as described in Brunner et al.[29]. Briefly the temporal traces were extracted by averaging the rCBV signal in the primary somatosensory barrel-field cortex (S1BF) for the ischemia and the retrosplenial granular cortex (RSGc) for detecting the SDs, both located in the left hemisphere. This procedure allowed to measure the occurrence of SDs over the recording period. Live recording of ischemia and spreading depolarizations can be visualized in **Movie 1**.

Activity maps

Pre- and post-stroke recordings are reshaped in shorter 40-s sessions, i.e., 50 frames, and averaged based on the whisker stimulation paradigm (left or right). In each voxel, we compared signals along the recording in a time window before the stimulus onset and a time window after stimulus onset using two-tailed Wilcoxon rank sum test. We obtained the z-statistics of the test for each voxel, and consequently a z-score for the coronal cross-section. Mean activity maps for left or right whisker stimulation (**Figure 3B** and **4A**) show z-score value calculated using a Fisher's transform for all voxels across the coronal cross-section. Only voxels with a z-score>1.6 were considered significantly activated ($p<0.05$ for a one-tailed test).

Hemodynamic response time-courses

The relative hemodynamic time course ΔrCBV was computed for each brain regions (after registration and segmentation; **Figure 3C-D** and **4B**), as the rCBV change compared to baseline at each time point. No additional filtering was used, and no trial was removed from the analysis.

Statistical analysis

Average rCBV changes were compared with a two-way ANOVA and a Fisher's LSD test for multiple comparisons using GraphPad Prism 9.2.0.

Results

Real-time imaging of stroke induction in awake rats.

We first developed a dedicated procedure for real-time imaging of stroke induction and associated evoked functional deficits in awake head-fixed rats (**Figure 1A**). Each rat was subjected to two cranial windows accessing independently the distal branch of the left MCA (**Figure 1B**, Left) and the selected brain regions to image (**Figure 1B**, Right). The latter was performed between bregma -2 and -4mm allowing for jointly monitoring the bilateral thalamo-cortical circuits of the somatosensory whisker-to-barrel pathway, including the ventroposterior medial nucleus of the thalamus (VPM) and the primary somatosensory barrel-field cortex (S1BF). Moreover, the selected coronal cross-section includes the posterior nucleus of the thalamus (Po), the reticular nucleus of the thalamus, and the ventral part of the zona incerta known for relaying information related to whiskers[37,38], and also direct efferent projections from the S1BF to other cortical and subcortical regions[39]. Prior to imaging sessions, rats were extensively trained to accept comfortable restraints in the experimental apparatus (**Figure 1C**), suitable for fUS recording of brain functions and stroke induction under awake conditions. After data acquisition, the coronal cross-section was registered and segmented on a custom-developed digital rat atlas[29] to provide a dynamic view of the changes in perfusion induced either by the stroke or evoked activity.

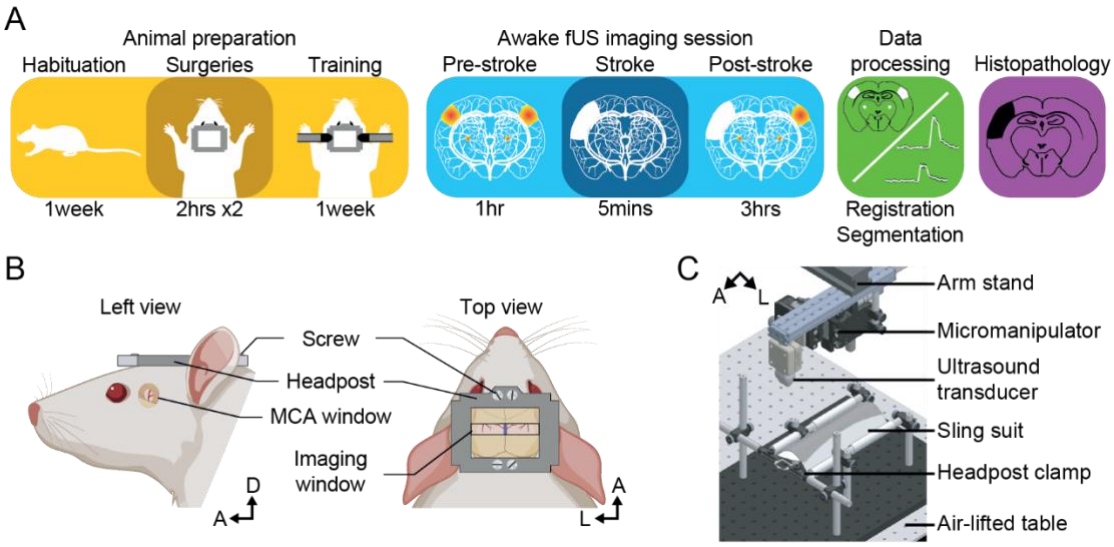

Figure 1. Experimental procedure.
(A) Workflow for brain imaging of awake head-fixed rats including, from left to right: animal preparation (habituation to the bench, implantation of cranial windows, training), functional ultrasound (fUS) imaging of stroke induction and brain functions, data processing, and histopathology. **(B)** Overview of the headpost implantation and cranial windows developed for combined MCAo (left) and brain imaging (right) under awake conditions. **(C)** Computer-aided design of the experimental apparatus where the animal is placed and secured in a suspended sling suit and the head fixed by the means of clamps holding the headpost implanted to the rat skull. A, Anterior; D, Dorsal; L, Left.

To overcome the limitations of conventional stroke models, we occluded the distal branch of the MCA by the mean of a chemo-thrombotic ferric chloride solution ($FeCl_3$)[30,31] while performing fUS imaging in awake rats (**Figure 2A**). It should be mentioned that the rats did not show any obvious signs of pain or discomfort (e.g., vocalization, aggressiveness) during the restrain period and occlusion procedure. The MCA occlusion (MCAo) was captured live with fUS and confirmed by the large drop of signal, i.e., ischemia, localized in the cortex of the left hemisphere (**Figure 2B, C** and **Movie 1**) as shown with µDoppler image taken 3hrs and 5d after the stroke onset (dashed outline, **Figure 2B**, Top row). Bmode images accounting for the brain tissue echogenicity remain unchanged early after stroke onset (3hrs) while showing focal hyper-echogenicity (dashed outline, **Figure 2B**, Bottom row) lately after stroke onset (5d) as a marker of focal lesion[40]. The stroke-induced hemodynamic changes have been continuously recorded for up to 3hrs after stroke onset, registered and segmented into 69 regions (**Supplementary Figure 1**). We first extracted the average change in rCBV (ΔrCBV in %) in the S1BF cortex of the left hemisphere (blue region, **Figure 2B**) and detected an abrupt drop of rCBV down to ~40% of the baseline level after the occlusion of the MCA, followed by a progressive decrease of the rCBV to 30% of baseline level 3hrs after the stroke onset (**Figure 2C** and **Movie 1**). Second, we extracted the average rCBV change from a cortical region supplied by the anterior cerebral artery directly after the MCAo. The signal extracted from the retrosplenial granular cortex (RSGc; purple and black regions in **Figure 2B**) shows successive and transient increases of signal. It characterizes spreading depolarizations (SDs) in the left hemisphere (in purple; **Figure 2D** and **Movie 1**) while resulting in a slight and stable oligemia in the right hemisphere (in black; **Figure 2D**). SDs were observed in the peri-ischemic territory of all rats subjected to MCAo and occurred in an ostensibly random fashion (**Figure 2E**); however, SDs showed a similar

bell shape and time-course across animals (**Figure 2F**). On average, we detected 5 SDs per hour per rat. Finally, we stained brain slices 24hrs after MCAo and confirmed that $FeCl_3$-induced ischemia turned into tissue infarction (red delineation; **Figure 2G**).

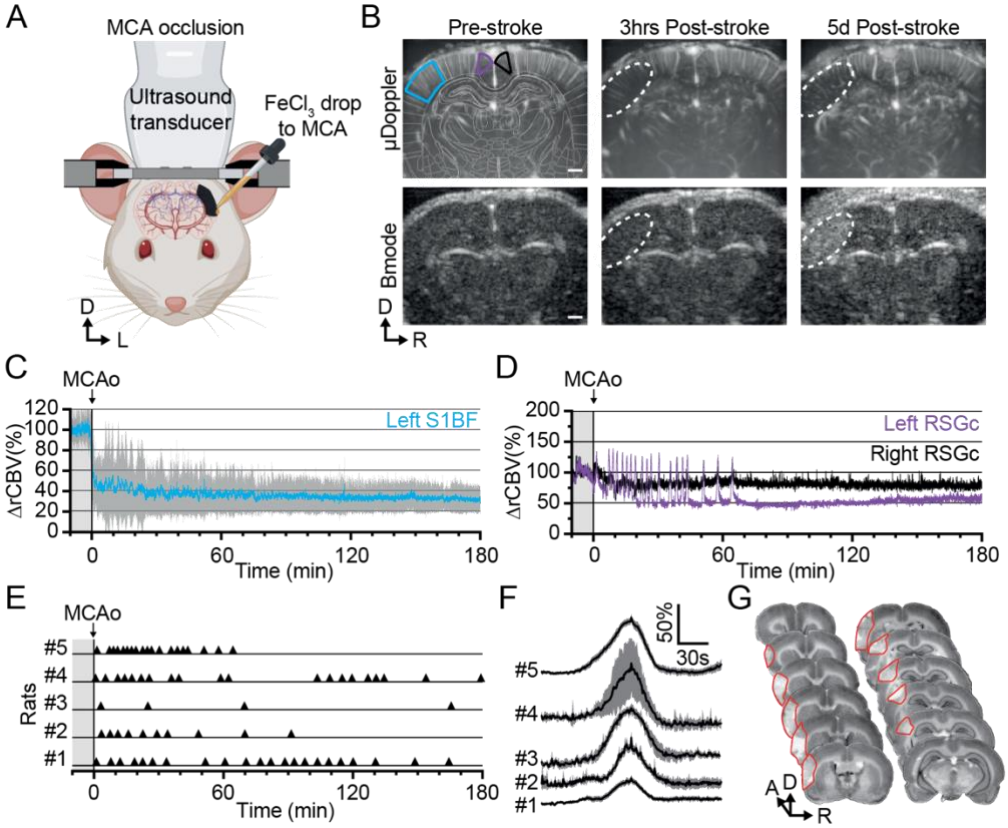

Figure 2. $FeCl_3$-stroke induction under awake conditions.
(A) Front view representation of functional ultrasound (fUS) imaging during live chemo-thrombosis of the left MCA with $FeCl_3$ in awake head-fixed rats. **(B)** Set of typical coronal µDoppler images of the brain microvasculature (top row) and morphological Bmode images (bottom row) before stroke (left), 3hrs (middle), and 5d after stroke onset (right) from the same animal. µDoppler images (top left) were registered and segmented based on a digital version of the rat brain atlas (white outlines). Colored outlines (cyan, purple, and black) delineate regions of interest plotted in (C) and (D). The white dotted region of interest highlights the ischemia in µDoppler images (Top row) and tissue hyper-echogenicity in Bmode (Bottom row). **(C)** Temporal plot of the average signal (ΔrCBV (%), mean±95%CI, n=5) in the barrel-field primary somatosensory cortex (S1BF, cyan) from the left hemisphere, affected by the MCAo. **(D)** Temporal plots of the average signal (ΔrCBV (%)) in the retrosplenial granular cortex (RSGc) from the affected (purple) and non-affected hemisphere (black) from the same animal. **(E)** Occurrence of spreading depolarizations after MCAo. Each horizontal line represents one rat; each triangle marker depicts the occurrence of one spreading depolarization. **(F)** Temporal plots of the average signal change (ΔrCBV (%), mean±95%CI) of the spreading depolarizations (centered on the peak) per rat. **(G)** Typical rat brain cross-sections stained by cresyl violet to evaluate the tissue infarction at 24hrs after $FeCl_3$-induction occlusion of MCA. The infarcted territory is delineated in red. Scale bars: 1mm. D: Dorsal; L: left; R: right.

Stroke-induced alterations of the thalamo-cortical functions.
One hour before and during 3hrs after the occlusion of the MCA, rats received mechanical stimulation of the whisker alternately delivered to the left and right pad using motorized combs (5-Hz sinusoidal deflection, 20° amplitude, 5-s duration; **Figure 3A**) to capture the spatiotemporal dynamics of the functional circuit. Before stroke, the sensory-evoked stimulations elicited a robust and statistically significant functional response (z-score>1.6, see Material and Methods) for both left and right stimulation (orange and green respectively; z-score maps; Pre-stroke panel, **Figure 3B** and **Movie 2**) with the activity spatially confined in the contralateral dorsal part of the VPM and S1BF. The temporal analysis of the somatosensory evoked responses in the contralateral hemisphere confirmed that VPM, Po, and S1BF regions were significantly activated and for both left and right stimuli (z-score, ****p<0.0001, ***p<0.001 and ****p<0.0001 respectively; Left panel, **Figure 3C**). We also detected significant increase of activity in S2, AuD, Ect (****p<0.0001) and PRh (***p<0.001) cortices and VPL nucleus (**p<0.01; the list of acronyms is provided in **Supplementary Table 2**), brain regions receiving direct efferent projections from the S1BF[39,41,42], VPM or Po nuclei[43–45]. It is worth noted that no habituation or sensitzation due to the repetitiveness of whiskers stimulation was observed in cortical and subcortical regions over the pre-stroke sessions (**Supplementary Figure 2**).

After the stroke, the activity map from the left pad stimulation elicited a similar response pattern as pre-stroke; however, the right pad stimulation showed a total absence of functional response in the S1BF cortex and a significant reduction of the response in the VPM (z-score maps; Post-stroke panel, **Figure 3B** and **Movie 2**). Over the 3hrs following stroke onset, functional responses to left whisker stimulation were still detected in the cortical and thalamic regions of the contralateral (right) hemisphere; however, functional responses to right whisker stimulation were only detected in subcortical nuclei (i.e., VPM, Po, VPL), while attenuated when compared with the responses from the pre-stroke period and from the other hemisphere (**Figure 3B, C**). Furthermore, no responses were detected at the cortical level (S1BF, S2, and AuD; right panel, **Figure 3B, C**).

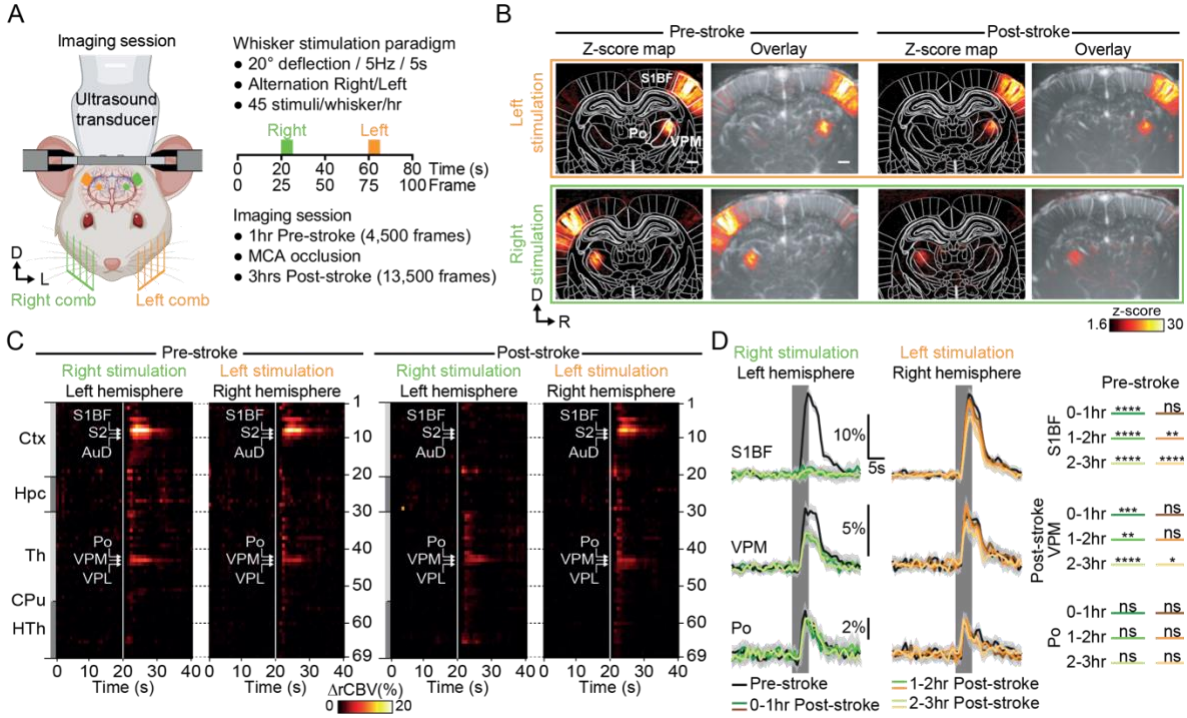

Figure 3. Early post-stroke alteration of whisker-to-barrel thalamo-cortical circuit.
(A) Front view representation of functional ultrasound (fUS) imaging during repetitive stimulation of the left (orange) or right whisker pad (green) with a mechanical comb in awake head-fixed rats. Whisker stimulations were delivered alternately between left and right whisker pads before and early after MCAo. Each rat receives 45 stimuli per whisker pad each hour of imaging. **(B)** Average activity maps (z-score) from one rat depicting evoked functional responses to either left (orange) or right whisker pads stimulation (green) registered with a digital version of the rat Paxinos atlas (white outlines) and overlaid with the corresponding coronal µDoppler image, before (left; Pre-stroke, average of 45 trials) and after stroke induction in the left hemisphere (right; Post-stroke, average of 125 trials). **(C)** Time-course traces of the average hemodynamic changes (ΔrCBV(%)) in response to right (green) or left whisker stimulation (orange) extracted from the contralateral hemisphere (left and right, respectively) before (left; Pre-stroke, n=5, 45 trials/rat) and after stroke induction in the left hemisphere (right; Post-stroke, n=5, 135 trials/rat). Brain regions are ordered by major anatomical structures (see **Supplementary Table 2**). The vertical line represents the stimulus start. S1BF, S2, AuD, VPM, VPL and Po regions are brain regions significatively activated (all pvalue<0.01). **(D)** Left, Average response curves from the S1BF, the VPM, and Po regions before (Pre-stroke, black, n=5, 45 trials/rat), and from first to third hour after stroke induction (0-1hr, 1-2hr, 2-3hr Post-stroke, orange and green, n=5, 45 trials/hr/rat). Data are mean±95%CI. The vertical bar represents the whisker stimulus. Right, Statistical comparison between pre-stroke and post-stroke response curves for S1BF, VPM, and Po regions (Two-way ANOVA with Fisher's LSD test for multiple comparisons; ns: non-significant; *p<0.05; **p<0.01; ***p<0.001; ****p<0.0001). Scale bars: 1mm. D: Dorsal; L: left; R: right; Ctx: Cortex; Hpc: Hippocampus; Th: Thalamus; CPu: Caudate Putamen; HTh: Hypothalamus; S1BF: barrel-field primary somatosensory cortex; S2: Secondary somatosensory cortex; AuD: Dorsal auditory cortex; VPM: Ventral postero-medial nucleus of the thalamus; ; VPL: Ventral postero-lateral nucleus of the thalamus; Po: Posterior nucleus of the thalamus.

To better evaluate how the functional responses were affected by the stroke, we have divided the post-stroke recording period into 3 sections of 1hr each and compared them with the 1-hr pre-stroke period (**Figure 3D**). Temporal plots from the pre-stroke period showed robust increases in signal during the stimulus in S1BF, VPM, and Po regions and high consistency between left and right stimuli (black plots, **Figure 3D** and **Supplementary Figure 2**); fitting well the hemodynamic response functions as previously observed[13,46]. Indeed, the hemodynamic responses were characterized by a quick increase in signal during whisker stimulation reaching a peak after 4.0s at 18.2±1.3% (4.0s, 18.6±1.2%) of baseline level for S1BF, 4.0s at 4.6±0.5% (3.2s, 5.8±0.7%) for VPM, and 2.4s at 2.9±0.7% (3.2s,

4.0±0.8%) for Po from the left stimulation (right, respectively; mean±95%CI) before slowly returning to baseline level (black plots, **Figure 3D**).

During the first hour following the stroke onset, functional responses in the left hemisphere (i.e., ipsilesional) were abolished in the S1BF, S2, and AuD (0-1hr Post-stroke, ****pvalue<0.0001), significantly decreased in the VPM (0-1hr Post-stroke, ***pvalue<0.001), and unchanged in Po and VPL (0-1hr Post-stroke, ns; **Figure 3D**) when compared with the pre-stroke responses (Pre-stroke, black plots, **Figure 3D**). Over the two following hours (i.e., 1-2hr and 2-3hr Post-stroke), the hemodynamic responses captured in these regions remained similar as those detected during the first post-stroke hour (green plots, **Figure 3D**).

Regarding the right hemisphere (i.e., contralesional), the functional responses of S1BF and VPM were conserved during the first hour after the stroke onset (ns, 0-1hr Post-stroke; orange plots, **Figure 3D**). During the two following hours, signal changes in S1BF show a significant and progressive decrease of activity (1-2hr Post-stroke **pvalue<0.01, 2-3hr Post-stroke ****pvalue<0.0001; orange plots, **Figure 3D**; Similar observation were made for S2 and AuD) whereas responses in VPM remained stable during the second hour post-stroke (1-2hr, ns) before significantly decreasing during the third hour (2-3hr Post-stroke *pvalue<0.05; orange plots, **Figure 3D**). Finally, the functional responses in VPM and Po remained unchanged over the 3hrs following the stroke onset (bottom panel, **Figure 3D**).

Delayed alteration of the somatosensory thalamo-cortical pathway

A secondary objective of this work was to evaluate the fUS ability to identify potential delayed functional alteration within a few days after the initial injury. Two animals were imaged five days after the MCAo following the same experimental, stimulation, imaging, and processing conditions as for the early post-stroke session.

First, we used the vascular markers and the shape of the hippocampus[28] to find back the coronal cross-section imaged during the pre-stroke session. Five days after the MCA occlusion, the functional responses to left whisker stimulation were still detected in the right hemisphere (i.e., contralesional), at the cortical and subcortical levels (orange; **Figure 4A**). As for the early post-stroke imaging period, the functional responses to right whisker stimulation were only detected in the subcortical nuclei and not at the cortical level (green; **Figure 4A**).

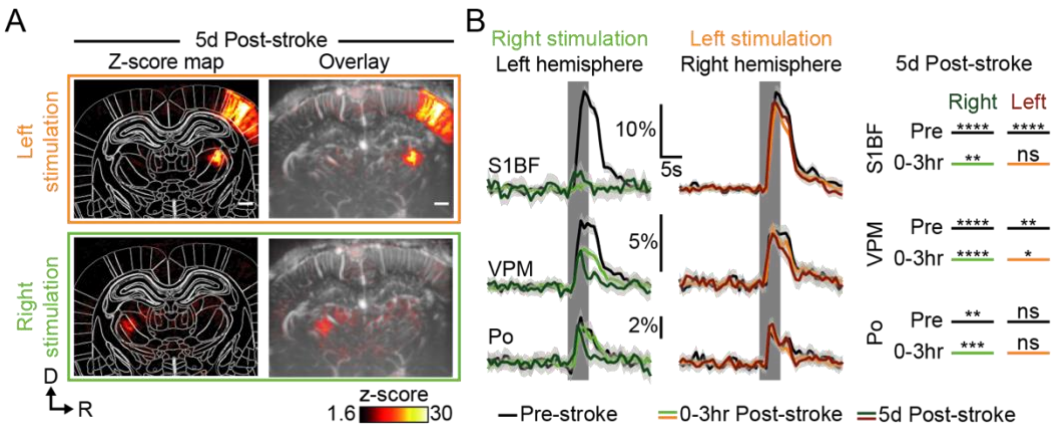

Figure 4. Late post-stroke alteration of whisker-to-barrel thalamo-cortical circuit.
(A) Activity maps (z-score; average of 45 trials) depicting evoked functional responses to left (orange) or right whisker pads stimulation (green) 5d after stroke induction. Z-score maps are registered with the Paxinos atlas (white outlines; Left) and overlaid with the corresponding coronal µDoppler image (Right). **(B)** Left; Average response curves to left and right whisker stimulation (orange and green; respectively) extracted from S1BF, VPM, and Po before (Pre-stroke, black, n=2, 45 trials/rat), 0-3hr (0-3hr Post-Stroke; light orange/green, n=2, 45 trials/hr/rat) and 5d after stroke induction (5d Post-stroke, dark orange/green, n=2, 45 trials/rat). Data are mean±95%CI. The vertical bar represents the whisker stimulus. Right; Statistical comparison between response curves for S1BF, VPM, and Po pre-stroke, 0-3hr and 5d post-stroke (Two-way ANOVA with Fisher's LSD test for multiple comparisons; ns: non-significant; *p<0.05; **p<0.01; ***p<0.001; ****p<0.0001). Scale bars: 1mm. D: Dorsal; R: right; S1BF: barrel-field primary somatosensory cortex; VPM: Ventral postero-medial nucleus of the thalamus; Po: Posterior nucleus of the thalamus.

Second, we extracted and compared the temporal plots of the functional responses gathered 5d after the stroke with the one obtained from the same two animals at the pre-stroke and 3hrs post-stroke timepoints (**Figure 4B**). At this later time point, the functional responses in the left S1BF (dark green plot, left panel, **Figure 4B.** Similar observation were made for the S2 and AuD) remained abolished when compared with the pre-stroke period (black plot; ****pvalue<0.0001), while slightly increased when

compared with the 3hrs post-stroke timepoint (green plot; **pvalue<0.01). The responses detected in the VPM 5d after the stroke onset (dark green plot, left panel, **Figure 4B**) were largely decreased not only when compared with the pre-stroke signal (black plot; ****pvalue<0.0001) but also with the 3hrs post-stroke trace (green plot; ****pvalue<0.0001). Interestingly, both the amplitude and time-to-peak of the hemodynamic response function were very similar to those from the early post-stroke signal (i.e., 3hrs post-stroke); however, the post-peak period was largely dampened in the 5d post-stroke signal. A similar alteration of the hemodynamic response function was also observed for the 5d post-stroke signal extracted from the Po nucleus when compared to the pre-stroke and 3hrs post-stroke signals (**pvalue<0.01 and ***pvalue<0.001, respectively; left panel, **Figure 4B.** Similar observation were made for the VPL).

Regarding the right hemisphere (i.e., non-ischemic; right panel, **Figure 4B**), the S1BF functional responses to left whisker stimulation were still significantly reduced when compared with pre-stroke responses (black plot, ****pvalue<0.0001) but remained similar to the traces detected at 3-hr post-stroke (orange plot, non-significant). As for the left VPM, both the amplitude and time-to-peak of the hemodynamic responses from the right VPM responses were consistent with pre-stroke and 3hr post-stroke values but the post-peak signal was decreased (brown plot, *pvalue<0.05 and **pvalue<0.01 respectively). The functional responses extracted from the Po and VPL did not show significant changes when compared to pre-stroke and 3hrs post-stroke responses.

Discussion

With this proof-of-concept study, we document on the feasibility of the continuous brain hemodynamics recording of a focal cerebral ischemia after MCAo in conscious rats. Using functional ultrasound imaging, we were able to extract multiple parameters (i.e., ischemia, location and spreading depolarization), characteristic of such cortical stroke. Then, we report on how the functional sensorimotor thalamo-cortical circuit was altered at early and late post-stroke stages.

Compared to highly-invasive conventional strategies such as clipping or suturing[1,2], the $FeCl_3$ model used here, is well suited to study stroke under awake conditions. Indeed, the use of $FeCl_3$ requires less manipulation, allows to maintain the dura intact and strongly reduces the risk of hemorrhage[30,31] and animal loss. Furthermore, the $FeCl_3$ model closely mimics key human stroke features including focal ischemia, creation of blood clot, possibility of vessel recanalization, and penumbral tissue[30,31].

The $FeCl_3$-induced MCAo showed an abrupt and massive drop of blood perfusion remaining constant during the entire recording period. The ischemia was confined within the cortical territory perfused by the MCA (**Figure 2B**), and the infarct (location and size; **Figure 2G**) is in agreement with previous observations[29,31]. We also detected transient hyperemic events associated with spreading depolarizations (SDs) within the peri-ischemic territory, with occurence, frequency and amplitude of the hemodynamic waves (**Figure 2D-F**) consistent with prior observation[29,47–52]. Moreover, the spatiotemporal dynamic of the $FeCl_3$-induced MCAo is consistent with previous fUS imaging reports on cortical ischemia with various stroke models[13,29,53].

On top of tracking large hemodynamic variation (i.e. ischemia, SDs), one asset of the fUS imaging technology relies on its ability to track subtle hemodynamic changes in sparse brain[13,23–28]. Therefore, we have evaluated how evoked functional responses reorganize at early and late timepoints after stroke induction. Functional responses to mechanical whisker stimulation were detected in several regions relaying the information from the whisker to the cortex, including the VPM and Po nuclei of the thalamus, and S1BF, the somatosensory barrel-field cortex. Responses were also observed in the S2 cortex involved in the multisensory integration of the information[37,38,54], the auditory cortex as it receives direct efferent projection from S1BF[39,54], and the VPL nuclei of the thalamus connected via corticothalamic projections[39].

Functional responses extracted in the left hemisphere affected by the focal ischemia (i.e., ipsilesionel) show a primary alteration of the whisker-to-barrel pathway within the first hour after the stroke onset. While the abrupt loss in S1BF responses was mainly driven by the focal ischemia, the immediate but partial drop in VPM responses (**Figure 3D**) might result from the direct the loss of the excitatory corticothalamic feedback to the VPM[45,55,56]. The absence of such cortical feedback suggests that the dampened functional responses might be driven by the intrinsic activity of the VPM in response to whisker stimulation. Five days after the initial injury, nuclei of the thalamus (VPM and Po) were subjected to a delayed and robust functional alteration (**Figure 4B**), probably associated with diaschisis, as previously characterised by tissue staining, reduction of metabolism, and perfusion[18–20,43]. Functional responses of the S1BF extracted from the right hemisphere (i.e., contralesionel) show a significant decrease shortly after the stroke onset (**Figure 3D**), and still detected at day 5, could be provoked by a loss of transcortical excitability[57,58]. The late drop in VPM responses might be explained by corticothalamic modulation of the projections toward VPM[37,58].

Further work will need to dissect the complex and long-lasting post-stroke alterations of the functional whisker-to-barrel pathway, including at the neuronal level, as fUS only reports on hemodynamics as a proxy of local neuronal activity[24,26,59–61]. Another limitation relies on the experimental condition as our brain imaging paradigm was constrained to a single cross-section, thus missing out-of-plane brain regions also affected by the stroke (e.g., ischemic size, infract extension, origin, and propagation pattern of SDs34) or involved in the whisker network (e.g., superior colliculus, striatum, amygdala and cerebellum)38. To overcome such limitation, one can extend the size of the cranial window to allow for larger scale imaging either by sequentially scanning the brain[26,28,29,53,59,60,62], or by using the recently developed volumetric fUS which provides whole-brain imaging capabilities in anesthetized[63] and awake rats[27].

Beyond studying the whisker-to-barrel somatosensory circuit, the brain-wide capability of fUS opens the door to investigate on stroke-affected brain circuits and functions using transgenic lines combined with opto-/chemo-genetic strategies as the technology is fully mature for mice studies[26–28,60].

Supplementary Materials

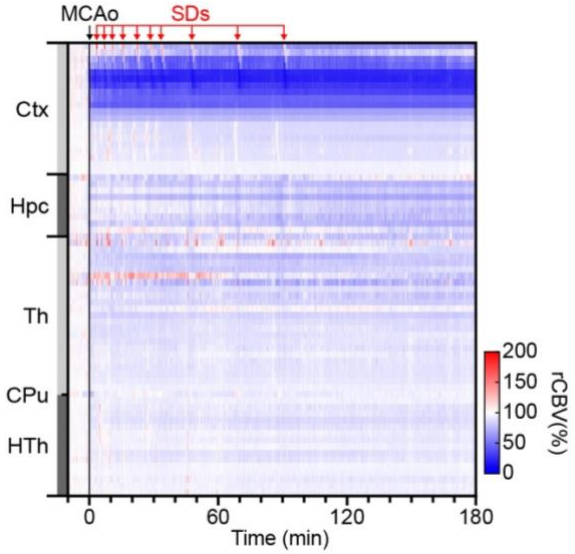

Supplementary Figure 1. Example of hemodynamic changes (rCBV in %) induced by MCAo in 69 regions located in the ischemic hemisphere of the imaged coronal cross-section. Regions are organized by main anatomical structures (see **Supplementary Table 2**). SDs stands for spreading depolarizations.

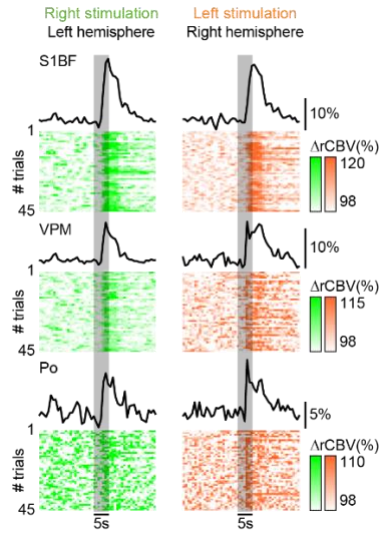

Supplementary Figure 2. Averaged hemodynamic response curves (ΔrCBV in %) of 45 consecutive right (green) or left whisker stimulation (orange; 1hr recording) extracted in the contralateral S1BF, VPM and Po regions (top to bottom). The corresponding individual trials presented below confirmed the stability across the recording. Vertical grey bar, the period of whisker stimulation.

	Imaging sessions						
Animal Tag	Control	Baseline (1hr)	Stroke	Early Post-Stroke (3hrs)	Late Post-Stroke (1hr)	Status	Issue
Rat1						Excluded - Miss functional responses from VPM and Po nuclei of the Thalamus	Imaging plane was too anterior
Rat2						Excluded - Unconsistency of functional responses during baseline	Issue with cranial window
Rat3						Included	
Rat4						Included	
Rat5						Included	
Rat6					+ 5d	Included	
Rat7						Included	
Rat8	2d before stroke				+ 5d	Included	
Rat9	2d before stroke					Control session: Included Stroke session: Excluded	Reperfusion of the MCA after stroke onset

Supplementary Table 1. Reporting on animal use, experimentation, inclusion/exclusion criteria, and figure association.

Region Number	Region Abbreviation	Name of the region
		Cortex (Ctx)
1	RSGc	Retrosplenial granular cortex, c region
2	RSD	Retrosplenial dysgranular cortex
3	M2	Secondary motor cortex
4	MPtA	Medial parietal association cortex
5	LPtA	Lateral parietal association cortex
6	S1Tr	Primary somatosensory cortex, trunk region
7	S1DZ	Primary somatosensory cortex, dysgranular zone
8	S1BF	Primary somatosensory cortex, barrel field
9	S2	Secondary somatosensory cortex
10	AuD	Secondary auditory cortex, dorsal area
11	Au1	Primary auditory cortex
12	AuV	Secondary auditory cortex, ventral area
13	Ect	Ectorhinal cortex
14	PRh	Perirhinal cortex
15	DLEnt	Dorsolateral entorhinal cortex
16	DEn	Dorsal endopiriform nucleus
17	Pir	Piriform cortex
18	RAPir	Rostral amygdalopiriform area
19	PLCo	Posterolateral cortical amygdaloid nucleus
20	PMCo	Posteromedial cortical amygdaloid nucleus
		Hippocampus (HPC)
21	DLG	Dorsal lateral geniculate nucleus
22	CA2	Field CA2 of the hippocampus
23	GrDG	Granular layer of the dentate gyrus
24	LMol	Lacunosum moleculare layer of the hippocampus
25	MoDG	Molecular layer of the dentate gyrus
26	PoDG	Polymorph layer of the dentate gyrus
27	FC	Fasciola cinereum
28	Py	Pyramidal cell layer of the hippocampus
29	SLu	Stratum lucidum of the hippocampus
		Thalamus (TH) 1/2
30	LDVL	Laterodorsal thalamic nucleus, ventrolateral part
31	LPMR	Lateral posterior thalamic nucleus, mediorostral part
32	MDL	Mediodorsal thalamic nucleus, lateral part
33	MDC	Mediodorsal thalamic nucleus, central part
34	MDM	Mediodorsal thalamic nucleus, medial part
35	OPC	Oval paracentral thalamic nucleus

Region Number	Region Abbreviation	Name of the region
		Thalamus (TH) 2/2
36	MHb	Medial habenular nucleus
37	LHb	Lateral habenular nucleus
38	PC	Paracentral thalamic nucleus
39	PVP	Paraventricular thalamic nucleus, posterior part
40	IMD	Intermediodorsal thalamic nucleus
41	CL	Centrolateral thalamic nucleus
42	Po	Posterior thalamic nuclear group
43	VPM	Ventral posteromedial thalamic nucleus
44	VPL	Ventral posterolateral thalamic nucleus
45	Rt	Reticular thalamic nucleus
46	VM	Ventromedial thalamic nucleus
47	Rh	Rhomboid thalamic nucleus
48	Re	Reuniens thalamic nucleus
49	Sub	Submedius thalamic nucleus
50	VRe	Ventral reuniens thalamic nucleus
51	ZID	Zona incerta, dorsal part
52	ZIV	Zona incerta, ventral part
53	STh	Subthalamic nucleus
		Striatum (STR)
54	CPu	Caudate putamen
		Hypothalamus (HTH)
55	SubI	Subincertal nucleus
56	A11	A11dopamine cells
57	A13	A13 dopamine cells
58	PHD	Posterior hypothalamic area, dorsal part
59	DA	Dorsal hypothalamic area
60	DMC	Dorsomedial hypothalamic nucleus, compact part
61	DMD	Dorsomedial hypothalamic nucleus, dorsal part
62	DMV	Dorsomedial hypothalamic nucleus, ventral part
63	PeFLH	Perifornical part of lateral hypothalamus
64	PeF	Perifornical nucleus
65	PLH	Peduncular part of lateral hypothalamus
66	VMHSh	Ventromedial nucleus of the hypothalamus shell
67	ArcL	Arcuate hypothalamic nucleus, lateral part
68	ArcD	Arcuate hypothalamic nucleus, dorsal part
69	ArcM	Arcuate hypothalamic nucleus, medial part

Supplementary Table 2. List of the 69 brain regions/hemisphere from the coronal cross-section µDoppler imaged in each rat organized by main anatomical structures. Adapted from the Paxinos rat brain atlas[35].

Movie 1. Movie of hemodynamic changes induced by MCA occlusion using $FeCl_3$ in awake head-fixed rats. Raw images.

Movie 2. Movie of thalamo-cortical functional responses to left and right whisker stimulation before and 3hrs after stroke onset.

Author contribution

	Brunner	Montaldo	Urban
Concept	X		
Methodology	X		
Software		X	X
Animal preparation	X		
Imaging	X		
Histochemistry	X		
Data Analysis	X	X	
Visualization	X		
Manuscript	X	X	X
Supervision		X	X
Funding			X

Funding

This work is supported by grants from the Fondation Leducq (15CVD02) and KU Leuven (C14/18/099-STYMULATE-STROKE). The functional ultrasound imaging platform is supported by grants from FWO (MEDI-RESCU2-AKUL/17/049, G091719N, and 1197818N), VIB Tech-Watch (fUSI-MICE), Neuro-Electronics Research Flanders TechDev fund (3D-fUSI project).

Acknowledgements

The authors thank the members of the Fondation Leducq network #15CVD02, Dr. M. Grillet, T. Lambert and lab members for their insightful comments and discussions. We thank NERF animal caretakers, including I. Eyckmans, F. Ooms, and S. Luijten, for their help with the management of the animals. Figures 1-3 use BioRender.com icons.

Competing interests

A.U. is the founder and a shareholder of AUTC company commercializing functional ultrasound imaging solutions for preclinical and clinical research.

References

1. MacRae, I. Preclinical stroke research - Advantages and disadvantages of the most common rodent models of focal ischaemia. *Br. J. Pharmacol.* **164**, 1062–1078 (2011).
2. Fluri, F., Schuhmann, M. K. & Kleinschnitz, C. Animal models of ischemic stroke and their application in clinical research. *Drug Des. Devel. Ther.* **9**, 3445–3454 (2015).
3. Sommer, C. J. Ischemic stroke: experimental models and reality. *Acta Neuropathologica* vol. 133 245–261 Preprint at https://doi.org/10.1007/s00401-017-1667-0 (2017).
4. Reimann, H. M. & Niendorf, T. The (Un)Conscious Mouse as a Model for Human Brain Functions: Key Principles of Anesthesia and Their Impact on Translational Neuroimaging. *Front. Syst. Neurosci.* **14**, 1–42 (2020).
5. Masamoto, K. & Kanno, I. Anesthesia and the Quantitative Evaluation of Neurovascular Coupling. *J. Cereb. Blood Flow Metab.* **32**, 1233–1247 (2012).
6. Traystman, R. J. Effect of anesthesia in stroke models. in *Neuromethods* 121–138 (Humana Press, 2010).
7. Hoffmann, U., Sheng, H., Ayata, C. & Warner, D. S. Anesthesia in Experimental Stroke Research. *Transl. Stroke Res.* **7**, 358–367 (2016).
8. Seto, A. *et al.* Induction of ischemic stroke in awake freely moving mice reveals that isoflurane anesthesia can mask the benefits of a neuroprotection therapy. *Front. Neuroenergetics* **6**, (2014).
9. Lu, H. *et al.* Induction and imaging of photothrombotic stroke in conscious and freely moving rats. *J. Biomed. Opt.* **19**, 096013 (2014).
10. Balbi, M. *et al.* Targeted ischemic stroke induction and mesoscopic imaging assessment of blood flow and ischemic depolarization in awake mice. *Neurophotonics* **4**, 035001 (2017).
11. Sunil, S. *et al.* Awake chronic mouse model of targeted pial vessel occlusion via photothrombosis. *Neurophotonics* **7**, 015005 (2020).
12. Mohajerani, M. H., Aminoltejari, K. & Murphy, T. H. Targeted mini-strokes produce changes in interhemispheric sensory signal processing that are indicative of disinhibition within minutes. *Proc. Natl. Acad. Sci. U. S. A.* **108**, E183-91 (2011).
13. Brunner, C. *et al.* Evidence from functional ultrasound imaging of enhanced contralesional microvascular response to somatosensory stimulation in acute middle cerebral artery occlusion/reperfusion in rats: A marker of ultra-early network reorganization? *J. Cereb. Blood Flow Metab.* **38**, 1690–1700 (2018).
14. Dijkhuizen, R. M. *et al.* Functional magnetic resonance imaging of reorganization in rat brain after stroke. *Proc. Natl. Acad. Sci. U. S. A.* **98**, 12766–12771 (2001).
15. Dijkhuizen, R. M. *et al.* Correlation between brain reorganization, ischemic damage, and neurologic status after transient focal cerebral ischemia in rats: a functional magnetic resonance imaging study. *J. Neurosci.* **23**, 510–517 (2003).
16. Abo, M., Chen, Z., Lai, L. J., Reese, T. & Bjelke, B. Functional recovery after brain lesion--contralateral neuromodulation: an fMRI study. *Neuroreport* **12**, 1543–1547 (2001).
17. Weber, R. *et al.* Early prediction of functional recovery after experimental stroke: functional magnetic resonance imaging, electrophysiology, and behavioral testing in rats. *J. Neurosci.* **28**, 1022–1029 (2008).
18. Zhang, J., Zhang, Y., Xing, S., Liang, Z. & Zeng, J. Secondary neurodegeneration in remote regions after focal cerebral infarction: a new target for stroke management? *Stroke* **43**, 1700–1705 (2012).
19. Carrera, E. & Tononi, G. Diaschisis: past, present, future. *Brain* **137**, 2408–2422 (2014).
20. Cao, Z., Harvey, S. S., Bliss, T. M., Cheng, M. Y. & Steinberg, G. K. Inflammatory responses in the secondary thalamic injury after cortical ischemic stroke. *Front. Neurol.* **11**, 236 (2020).
21. Levy, H., Ringuette, D. & Levi, O. Rapid monitoring of cerebral ischemia dynamics using laser-based optical imaging of blood oxygenation and flow. *Biomed. Opt. Express* **3**, 777 (2012).
22. Dunn, A. K. Laser Speckle Contrast Imaging of Cerebral Blood Flow. *Ann. Biomed. Eng.* **40**, 367–377 (2012).
23. Macé, E. *et al.* Functional ultrasound imaging of the brain. *Nature methods* **8**, 662–664 (2011).
24. Urban, A. *et al.* Chronic assessment of cerebral hemodynamics during rat forepaw electrical stimulation using functional ultrasound imaging. *Neuroimage* **101**, 138–149 (2014).
25. Urban, A. *et al.* Real-time imaging of brain activity in freely moving rats using functional ultrasound. *Nature methods* **12**, 873–878 (2015).
26. Macé, É. *et al.* Whole-Brain Functional Ultrasound Imaging Reveals Brain Modules for Visuomotor Integration. *Neuron* **100**, 1241-1251.e7 (2018).
27. Brunner, C. *et al.* A Platform for Brain-wide Volumetric Functional Ultrasound Imaging and Analysis of Circuit Dynamics in Awake Mice. *Neuron* (2020) doi:10.1016/j.neuron.2020.09.020.
28. Brunner, C. *et al.* Whole-brain functional ultrasound imaging in awake head-fixed mice. *Nat. Protoc.* (2021) doi:10.1038/s41596-021-00548-8.
29. Brunner, C. *et al.* Brain-wide continuous functional ultrasound imaging for real-time monitoring of hemodynamics during ischemic stroke. (2022) doi:10.1101/2022.01.19.476904.

30. Karatas, H. *et al.* Thrombotic distal middle cerebral artery occlusion produced by topical FeCl(3) application: a novel model suitable for intravital microscopy and thrombolysis studies. *J. Cereb. Blood Flow Metab.* **31**, 1452–1460 (2011).
31. Syeara, N. *et al.* Motor deficit in the mouse ferric chloride-induced distal middle cerebral artery occlusion model of stroke. *Behav. Brain Res.* **380**, 112418 (2020).
32. Percie du Sert, N. *et al.* The ARRIVE guidelines 2.0: Updated guidelines for reporting animal research. *PLoS Biol.* **18**, e3000410 (2020).
33. Martin, C., Martindale, J., Berwick, J. & Mayhew, J. Investigating neural–hemodynamic coupling and the hemodynamic response function in the awake rat. *Neuroimage* **32**, 33–48 (2006).
34. Topchiy, I. A. *et al.* Conditioned lick behavior and evoked responses using whisker twitches in head restrained rats. *Behav. Brain Res.* **197**, 16–23 (2009).
35. Paxinos, G. *The rat brain in stereotaxic coordinates*. (Academic Press, 2014).
36. ClemBrunner & nerf-common. *nerf-common/whole-brain-fUS: whole-brain-fUS v1.0*. (2021). doi:10.5281/zenodo.4585348.
37. Adibi, M. Whisker-mediated touch system in rodents: From neuron to behavior. *Front. Syst. Neurosci.* **13**, 40 (2019).
38. Bosman, L. W. J. *et al.* Anatomical pathways involved in generating and sensing rhythmic whisker movements. *Front. Integr. Neurosci.* **5**, 53 (2011).
39. Zakiewicz, I. M., Bjaalie, J. G. & Leergaard, T. B. Brain-wide map of efferent projections from rat barrel cortex. *Front. Neuroinform.* **8**, 5 (2014).
40. Gómez-de Frutos, M. C. *et al.* B-mode ultrasound, a reliable tool for monitoring experimental intracerebral hemorrhage. *Front. Neurol.* **12**, 771402 (2021).
41. Fabri, M. & Burton, H. Ipsilateral cortical connections of primary somatic sensory cortex in rats. *J. Comp. Neurol.* **311**, 405–424 (1991).
42. Frostig, R. D., Xiong, Y., Chen-Bee, C. H., Kvasnák, E. & Stehberg, J. Large-scale organization of rat sensorimotor cortex based on a motif of large activation spreads. *J. Neurosci.* **28**, 13274–13284 (2008).
43. Viaene, A. N., Petrof, I. & Sherman, S. M. Properties of the thalamic projection from the posterior medial nucleus to primary and secondary somatosensory cortices in the mouse. *Proc. Natl. Acad. Sci. U. S. A.* **108**, 18156–18161 (2011).
44. El-Boustani, S. *et al.* Anatomically and functionally distinct thalamocortical inputs to primary and secondary mouse whisker somatosensory cortices. *Nat. Commun.* **11**, 3342 (2020).
45. Landisman, C. E. & Connors, B. W. VPM and PoM nuclei of the rat somatosensory thalamus: intrinsic neuronal properties and corticothalamic feedback. *Cereb. Cortex* **17**, 2853–2865 (2007).
46. Hirano, Y., Stefanovic, B. & Silva, A. C. Spatiotemporal evolution of the functional magnetic resonance imaging response to ultrashort stimuli. *J. Neurosci.* **31**, 1440–1447 (2011).
47. Nakamura, H. *et al.* Spreading depolarizations cycle around and enlarge focal ischaemic brain lesions. *Brain* **133**, 1994–2006 (2010).
48. Takeda, Y., Zhao, L., Jacewicz, M., Pulsinelli, W. A. & Nowak, T. S., Jr. Metabolic and perfusion responses to recurrent peri-infarct depolarization during focal ischemia in the Spontaneously Hypertensive Rat: dominant contribution of sporadic CBF decrements to infarct expansion. *J. Cereb. Blood Flow Metab.* **31**, 1863–1873 (2011).
49. Bere, Z., Obrenovitch, T. P., Kozák, G., Bari, F. & Farkas, E. Imaging reveals the focal area of spreading depolarizations and a variety of hemodynamic responses in a rat microembolic stroke model. *J. Cereb. Blood Flow Metab.* **34**, 1695–1705 (2014).
50. Farkas, E., Pratt, R., Sengpiel, F. & Obrenovitch, T. P. Direct, live imaging of cortical spreading depression and anoxic depolarisation using a fluorescent, voltage-sensitive dye. *J. Cereb. Blood Flow Metab.* **28**, 251–262 (2008).
51. Farkas, E., Bari, F. & Obrenovitch, T. P. Multi-modal imaging of anoxic depolarization and hemodynamic changes induced by cardiac arrest in the rat cerebral cortex. *Neuroimage* **51**, 734–742 (2010).
52. Bogdanov, V. B. *et al.* Susceptibility of primary sensory cortex to spreading depolarizations. *J. Neurosci.* **36**, 4733–4743 (2016).
53. Hingot, V. *et al.* Early Ultrafast Ultrasound Imaging of Cerebral Perfusion correlates with Ischemic Stroke outcomes and responses to treatment in Mice. *Theranostics* **10**, 7480–7491 (2020).
54. Lohse, M., Dahmen, J. C., Bajo, V. M. & King, A. J. Subcortical circuits mediate communication between primary sensory cortical areas in mice. *Nat. Commun.* **12**, 3916 (2021).
55. Temereanca, S. & Simons, D. J. Functional topography of corticothalamic feedback enhances thalamic spatial response tuning in the somatosensory whisker/barrel system. *Neuron* **41**, 639–651 (2004).
56. Bourassa, J., Pinault, D. & Deschênes, M. Corticothalamic projections from the cortical barrel field to the somatosensory thalamus in rats: A single-fibre study using biocytin as an anterograde tracer. *Eur. J. Neurosci.* **7**, 19–30 (1995).

57. Rema, V. & Ebner, F. F. Lesions of mature barrel field cortex interfere with sensory processing and plasticity in connected areas of the contralateral hemisphere. *J. Neurosci.* **23**, 10378–10387 (2003).
58. Li, L., Rema, V. & Ebner, F. F. Chronic suppression of activity in barrel field cortex downregulates sensory responses in contralateral barrel field cortex. *J. Neurophysiol.* **94**, 3342–3356 (2005).
59. Sieu, L.-A. *et al.* EEG and functional ultrasound imaging in mobile rats. *Nat. Methods* **12**, 831–834 (2015).
60. Sans-Dublanc, A. *et al.* Optogenetic fUSI for brain-wide mapping of neural activity mediating collicular-dependent behaviors. *Neuron* (2021) doi:10.1016/j.neuron.2021.04.008.
61. Nunez-Elizalde, A. O. *et al.* Neural basis of functional ultrasound signals. *bioRxiv* (2021) doi:10.1101/2021.03.31.437915.
62. Brunner, C. *et al.* Mapping the dynamics of brain perfusion using functional ultrasound in a rat model of transient middle cerebral artery occlusion. *J. Cereb. Blood Flow Metab.* **37**, 263–276 (2017).
63. Rabut, C. *et al.* 4D functional ultrasound imaging of whole-brain activity in rodents. *Nature methods* **16**, 994–997 (2019).